Luminescence and Amplified Stimulated Emission in CdSe–ZnS-Nanocrystal-Doped TiO2 and ZrO2 Waveguides

ARTICLE *in* ADVANCED FUNCTIONAL MATERIALS · JULY 2007

Impact Factor: 11.81 · DOI: 10.1002/adfm.200600955

7 AUTHORS, INCLUDING:

Raffaella Signorini
University of Padova
81 PUBLICATIONS **1,353** CITATIONS
SEE PROFILE

Alessandro Chiasera
Italian National Research Council
237 PUBLICATIONS **2,220** CITATIONS
SEE PROFILE

Maurizio Ferrari
Italian National Research Council
520 PUBLICATIONS **5,458** CITATIONS
SEE PROFILE

Alessandro Martucci
University of Padova
195 PUBLICATIONS **2,710** CITATIONS
SEE PROFILE

FULL PAPER

ADVANCED FUNCTIONAL MATERIALS

DOI: 10.1002/adfm.200600955

Luminescence and Amplified Stimulated Emission in CdSe–ZnS-Nanocrystal-Doped TiO_2 and ZrO_2 Waveguides**

By *Jacek Jasieniak*, *Jessica Pacifico*, *Raffaella Signorini*, *Alessandro Chiasera*, *Maurizio Ferrari*, *Alessandro Martucci*,* and *Paul Mulvaney**

A reproducible route for the preparation of high-quality CdSe–ZnS-doped titania and zirconia waveguides is presented. The optical properties of the resultant composite materials are found to be sensitive to the semiconducting properties of the host matrix. Titania-based composites are seen to be inherently photounstable because of photoelectron injection into the bulk matrix and subsequent nanocrystal (NC) oxidation. In comparison, zirconia composites are significantly more robust with high photoluminescence (PL) retained for annealing temperatures up to 300 °C. Both titania and zirconia composite waveguides exhibit amplified stimulated emission (ASE); however only zirconia-based waveguides exhibit long-term photostability (loss of less than 30 % ASE intensity after more than 40 min continuous excitation). We conclude that the low electron affinity of zirconia and its inherent high refractive index makes it an ideal candidate for NC-based optical waveguides.

1. Introduction

The transfer of nanocrystals (NCs) into sol–gel-based matrices provides a generic pathway for the development of complex materials with unique optical,[1,2] electronic,[3] or magnetic[4,5] signatures. Of particular interest at present is the possibility that NC-doped glasses could provide stable laser media with tunable emission wavelengths.[6–9] Through appropriate modification to the surface chemistry, it is possible to disperse semiconductor or metal NCs into inorganic matrices such as sol–gels,[10,11] or into polymeric environments.[12–14] However, the development of reliable dispersion methods have generally proved quite elusive. NCs typically aggregate or phase-separate in polymer-based matrices such as poly(methyl methacrylate) (PMMA) or lose their functional property (i.e., luminescence) rapidly upon exposure to the harsh environments of the matrix precursor solutions and during the polymerization steps. If dispersion is successful, consolidation of the resulting matrices at elevated temperatures once again leads to rapid loss of luminescence because of NC degradation.

Of additional consideration is the chemical nature of the host matrix, which can potentially govern the final material's refractive index. Inorganic sol–gel matrices therefore have an advantage over organic-based polymer hosts because of the high refractive indices that are achievable. Previous studies have shown that sol–gel waveguides can be easily fabricated owing to their high refractive index and that they typically exhibit optical propagation losses of less than 1 dB cm^{-1}.[15] Such sol–gel matrices have also been found to be excellent hosts for organic chromophores,[16,17] erbium cations,[18,19] and indeed quantum dots (QDs).[20–22] Truly optically 'photoluminescence (PL)-active' waveguides have been however ridden with obstacles. The main obstacle is the high annealing temperature needed to achieve densified materials. Erbium-based sol–gel waveguides are the exception to this rule as they require annealing temperatures greater than ca. 400 °C.[18] This factor has however largely restricted organic dyes and even QDs from being utilized in such waveguides. While preserving PL, the low annealing temperatures (150 °C or less) prevent significant condensation of the matrix, which for low nanoparticle volume fractions results in low-refractive-index materials. This may not be a problem for simple planar waveguide geometries, but ultimately for more complex structures such as Bragg reflectors[23] and microcavities,[18,24,25] which require high-refractive-index gradients between materials, this is an issue that needs to be resolved.

[*] Prof. A. Martucci, J. Jasieniak
Dipartimento di Ingegneria Meccanica Settore Materiali
Università di Padova
Via Marzolo, 9, 35131 Padova (Italy)
E-mail: alex.martucci@unipd.it
Prof. P. Mulvaney, J. Jasieniak, Dr. J. Pacifico
School of Chemistry
University of Melbourne
Parkville, VIC 3010 (Australia)
E-mail: mulvaney@unimelb.edu.au
Dr. R. Signorini
Dipartimento di Scienze Chimiche
Università di Padova
Via Marzolo, 1, 35131 Padova (Italy)
Dr. A. Chiasera, Dr. M. Ferrari
3CNR-IFN Istituto di Fotonica e Nanotecnologie
CSMFO group
Via Sommarive 14, 38050 Povo (Trento) (Italy)

[**] J.J. acknowledges receipt of an APA postgraduate stipend, an ARCNN travel scholarship, and the University of Melbourne's PORES overseas scholarship, provided to assist in overseas research in Padova, Italy. A.M. thanks the Universities of Melbourne and Padova for its support through the University academic-exchange program, and MIUR through the PRIN 2004 project. P.M. acknowledges the support of the ARC through DP Grant 0451651 and FF 0561486.

In this paper we discuss the fabrication, optical characterization, and functional stability of CdSe–ZnS QD waveguides prepared using both titania and zirconia as high-refractive-index host materials. Both chemical and photostability of the nanoparticles must be retained within the composite. Chemical stability is afforded by a robust inorganic shell (i.e., ZnS) with adequate surface passivation.[26] Photostability is highly dependent on the quality of the core/shell QD and the extent of potential carrier traps in its vicinity. These traps can be either on the surface of the QD,[27] at the core/shell interface,[28] or in the surrounding matrix itself.[29,30] The latter factor therefore implies that careful selection of a suitable host matrix is necessary to achieve stable QD composites. The two selected host matrices, TiO_2 and ZrO_2, have been specifically chosen because of their high refractive indices and the significant differences in their electron affinities and ionization potentials.[31,32] Titania may form a type-II structure depending on the CdSe QD size, whereas in contrast, zirconia acts solely as a type-I host for all CdSe QD sizes. This is illustrated in Scheme 1. In a type-I structure, the conduction and valence electrons in the dopant cannot in principle access the matrix because it is energetically unfeasible. However in a type-II structure, one of the charge carriers may escape. In Scheme 1 (b1), the electron can diffuse into the conduction band of the matrix, whereas in b2, the hole escapes into the matrix valence band. These processes may lead to permanent NC corrosion unless under steady-state illumination: the escaping charge carriers tend to recombine with the NCs. Little is known about the kinetics and efficiencies of these processes at present.

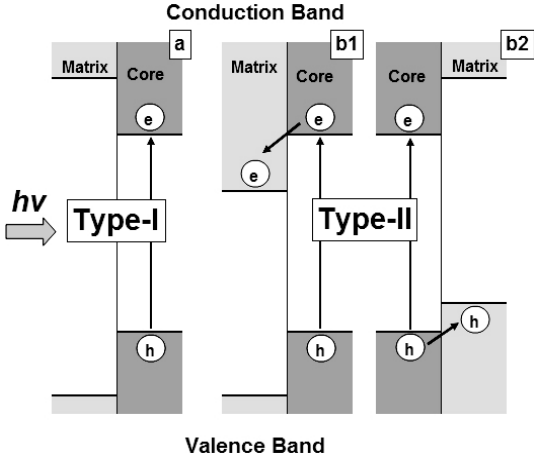

Scheme 1. The localization of the electron and hole carriers across a heterostructure interface in a type-I (a) and in a type-II (b1,2) configuration.

By comparing both matrices we find that a compromise between annealing temperature and PL quantum yield (QY) provides the best overall QD composite. Furthermore, using confocal microscopy and a standard 1D optical amplifier configuration, we show that stability of both spontaneous emission and amplified stimulated emission (ASE) of the composites is achievable, but is highly dependent on the host matrix.

2. Results and Discussion

2.1. CdSe–ZnS Composite Thin Films

The most common method to achieve homogeneous incorporation of nanoparticles into a variety of matrices is through the use of bifunctional ligands that provide a favorable interaction between the ligand environment and the medium. In Figure 1 we present the normalized absorbance and relative PL spectra of ca. 4.6 nm core-size CdSe–ZnS QDs with their native hydrophobic surface in $CHCl_3$, following 5-aminopentanol exchange in methanol (MeOH) and in the respective titania and zirconia sols. By comparing the first absorption peak at

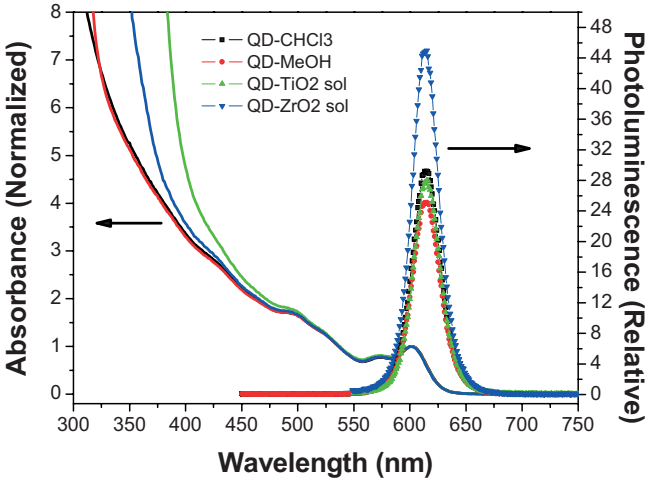

Figure 1. Absorption and relative fluorescence spectra of CdSe–ZnS nanoparticles in chloroform, ethanol, and in the titania and zirconia sols.

602 nm, it is clear that no spectral shift occurred during the $CHCl_3$–MeOH phase-transfer or upon incorporation of the QDs into the sols. This observation is typical of well-dispersed and colloidally stable samples. Two experimental factors made this possible: i) thorough ligand exchange and ii) the use of acetylacetone as the chelating agent for the Ti and Zr precursors. For the sample in Figure 1, the QY of the as-prepared QDs was ca. 0.29, as measured with respect to rhodamine 640. Only a slight decrease in the PL QY to ca. 0.24 was observed following the stabilization of the QDs in MeOH. When incorporated into the sol-solution we observed that the PL of QDs in the TiO_2 sol remained largely unchanged (ca. 0.28); however a slight increase in the PL was observed for the QDs in the ZrO_2 sol (ca. 0.45).

Following film deposition by spin-coating, transmission electron microscopy (TEM) was used to determine the homogeneity of the dispersed QDs in both titania and zirconia thin films. These results are displayed in Figure 2a and b for composites heat-treated at 100 °C. From these figures, it is clear that the QDs are homogeneously dispersed within both metal oxide matrices. This clearly indicates that the hydroxyl-rich surface environment provided by the 5-aminopentanol ligands allows

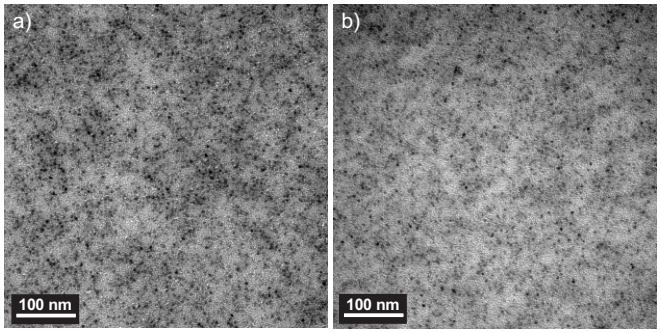

Figure 2. TEM images of CdSe–ZnS nanoparticles in titania (a) and zirconia (b) matrices following heat-treatment at 100 °C.

for effective condensation with the matrix following solvent evaporation. Tapping-mode atomic-force microscopy (AFM) imaging was utilized to determine the overall surface roughness, because this largely determines the extent of propagation losses of the confined optical modes. Figure 3 shows the 2D and 3D surface profiles of QD-doped films annealed at 300 °C. The root-mean-square roughness over a 2 μm × 2 μm region of the titania (Fig. 3a) and zirconia (Fig. 3b) composite films was found to be 3.5 and 0.9 nm, respectively. The equivalent roughness of the undoped films is typically found to be <2 nm, suggesting that the NC doping does not significantly reduce the smoothness of the spin-coated films.

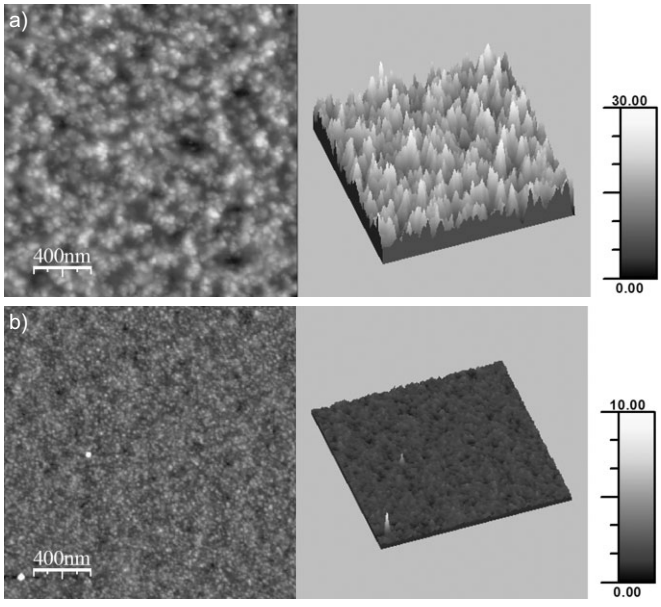

Figure 3. 2D and 3D surface profiles of CdSe–ZnS in titania (a) and zirconia (b) heat-treated at 300 °C as measured through tapping-mode AFM. Scale bar is displayed in units of nanometers.

2.2. Refractive Index of the Composites

The refractive index (n_g) and film thickness (d) as a function of annealing temperature for the two host matrices were measured by using spectroscopic ellipsometry. A Cauchy dispersion model was used to fit the raw data. The n_g values reported in Table 1 are at the standard spectral wavelength of 633 nm. Because of the low fill-factor of QDs in the sample (< 1 % by volume) an effective-medium model was not needed to account for the effect of the QD dispersion. The measured refractive indices for the samples are summarized in Figure 4. The difference in n_g following QD doping was minimal. Because of the condensation of the matrix, a significant increase in n_g and a concordant decrease in thickness was consistently observed with increasing annealing temperature. For example, following heat-treatment at only 100 °C, the average film refractive index n_g and thickness d of two thin films of TiO_2 and ZrO_2 were

Table 1. Summary of relevant parameters obtained for the TiO_2 and ZrO_2 doped and undoped thin films produced in this study.

Matrix	n_g	Film Thickness [nm]	Porosity [%]	Min d/λ_0 value for guiding
ZrO_2-100	1.554	262	51.09	0.308
ZrO_2-200	1.631	150	45.27	0.203
ZrO_2-300	1.755	82	35.90	0.131
ZrO_2-400	1.855	63	28.26	0.101
ZrO_2-500	1.921	53	23.15	0.088
ZrO_2-QD-100	1.601	81	47.53	0.234
ZrO_2-QD-200	1.683	56	41.35	0.165
ZrO_2-QD-300	1.753	39	36.05	0.132
ZrO_2-QD-400	1.794	30	32.93	0.118
ZrO_2-QD-500	1.829	27	30.26	0.108
TiO_2-100	1.681	119	51.69	0.167
TiO_2-200	1.813	76	43.98	0.112
TiO_2-300	1.916	60	37.93	0.089
TiO_2-400	1.967	55	34.91	0.08
TiO_2-500	2.052	48	29.83	0.069
TiO_2-QD-100	1.693	54	50.99	0.160
TiO_2-QD-200	1.849	37	41.87	0.103
TiO_2-QD-300	1.935	31	36.81	0.085
TiO_2-QD-400	1.963	27	35.15	0.081
TiO_2-QD-500	2.006	24	32.59	0.074

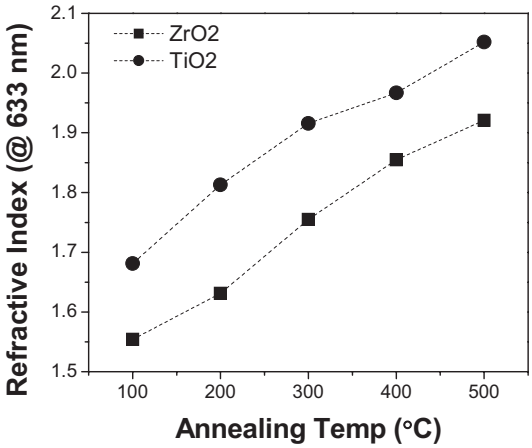

Figure 4. The change in refractive index of the titania and zirconia host matrices as a function of the annealing temperature. These values are all reported at 633 nm.

ADVANCED FUNCTIONAL MATERIALS

found to be 1.68 and 119 nm, and 1.55 and 262 nm, respectively, whereas after annealing at 300 °C these values changed to 1.94 and 60 nm, and 1.76 and 82 nm. We found that in general n_g of TiO_2 films were ca. 0.15 higher than ZrO_2 at each studied annealing temperature.

From the fitted refractive index profiles and the film thickness, an estimation of the porosity for each sample was calculated using the Bruggeman model of the effective medium[33]

$$Porosity = \left(\left(\frac{n_d^2 - n_g^2}{n_d^2 + 2n_g^2}\right) \Big/ \left(\frac{n_d^2 - n_g^2}{n_d^2 + 2n_g^2} - \frac{1 - n_g^2}{1 + 2n_g^2}\right)\right) 100\% \quad (1)$$

Here, n_d is the fully densified refractive index (anatase $TiO_2 = 2.52$,[34] tetragonal $ZrO_2 = 2.208$[35]) and n_g is the measured refractive index at the reference wavelength. The results in Table 1 reveal that the overall film porosity significantly decreased for both matrices at higher annealing temperatures. This is expected because of the structural changes that occur during heating (i.e., removal of residual solvent and organics, to hydroxyl condensation and structural relaxation).[36] The extent of densification of the ZrO_2 matrix was found to be very similar to that of the TiO_2 matrix at each studied annealing temperature. This similarity in densification rate led to the ZrO_2 matrix retaining a relatively high n_g value in comparison to TiO_2 at all the treatment temperatures studied here. This has significant implications when determining the critical thickness of a guiding layer in planar waveguide structures, and will be discussed shortly.

X-ray diffraction was also carried on all the thin films described here (not shown). Both matrices were amorphous at all annealing temperatures less than 400 °C. Following heat-treatment at 500 °C, however, the TiO_2 sample exhibited the expected anatase crystal phase, whereas the ZrO_2 exhibited the tetragonal crystal structure.

2.3. Matrix and Temperature Dependence of Composite Steady-State Photoluminescence

The homogeneity of the NCs within the matrix was assessed by using confocal microscopy. PL spectra were collected from different points on the films. To avoid complications created by photoinduced bleaching or photobrightening, exposure to the films was limited to <3 s per spectrum and spectra were taken at low intensity (ca. 0.4 kW cm^{-2}). The relative PL signals of the QDs in titania and zirconia thin films, measured at different annealing temperatures, are shown in Figure 5a and b, respectively. In both cases the relative PL decreased significantly with increasing annealing temperature. Little change in the PL peak position was observed for temperatures below 300 °C. Above this temperature however, significant blue-shifting occurred, and was accompanied by almost complete quenching of the PL signal, indicating that significant oxidation of the NC lattice had occurred.

The differences in luminescence efficiency between both composites was measured for films with the same NC volume fraction. Because the film thicknesses differed, this was accounted for through a simple linear scaling coefficient

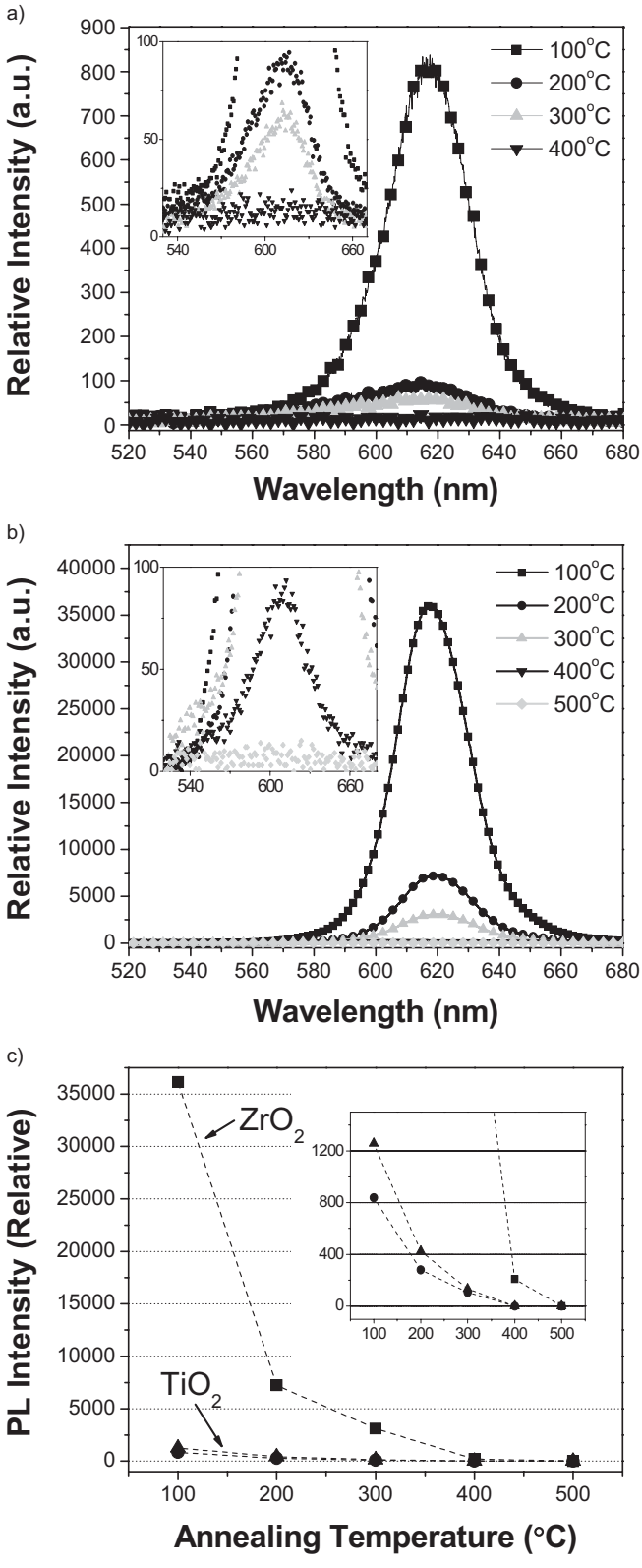

Figure 5. Relative decrease in PL following exposure to an increased annealing temperature of composites with a host matrix of a) titania and b) zirconia. c) The comparative PL signal between the TiO_2 (°) and ZrO_2-QD (■) composites. Included is the TiO_2-QD PL following a correction for film-thickness variation (▲).

(d_{ZrO_2}/d_{TiO_2}). We estimate that the differences in refractive index and hence reflection coefficient account for only a 5 % difference in the luminescence intensity, and that most of the differences are directly caused by intrinsic differences in the QY of the NCs in the two matrices. Indeed, the luminescence intensity varied by a factor of 20–30 for samples annealed at 300 °C and below. To explain this significant difference in PL intensity, we consider the possible charge-transfer processes in our composites. At present there is some ambiguity in the reported valence (E_{vb}) and conduction-band (E_{cb}) energy levels of CdSe in the literature. The reported E_{cb} values range between –4.7 and –2.0 eV versus vacuum.[37–42] There is evidently a size dependence of both E_{cb} and E_{vb}, which to zeroth order can be approximated by

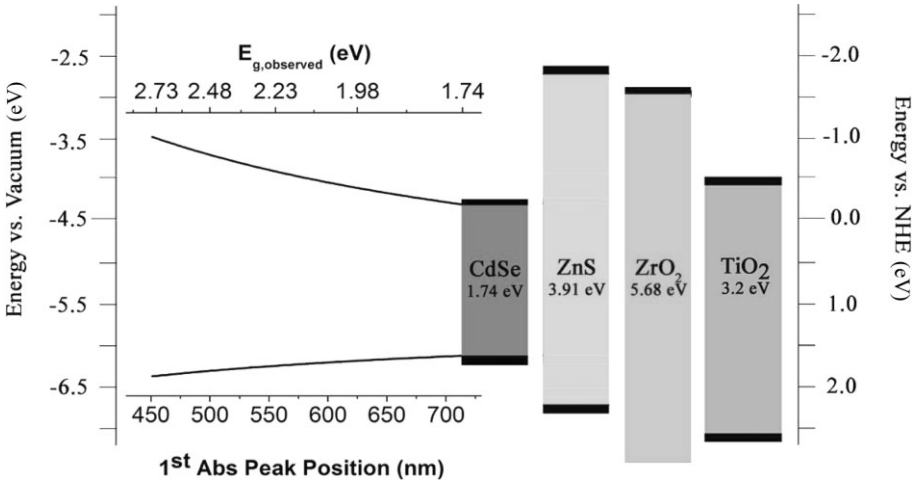

Figure 6. Summary of the electron affinities and ionization potentials of all composite components used in this paper and the relative change in conduction and valence-band energies (see Eq. 2) of CdSe as a function of the first absorption peak (nm). Because of the ambiguity of the reported values in literature, we utilize a bulk CdSe electron affinity –4.3 eV versus vacuum and an ionization potential of –6.04 versus vacuum. As discussed in the report we do not claim that these are absolute values.

$$E_{cb} = E_{cb,bulk} + \left(E_{g,observed} - E_{g,bulk}\right)\left(m_h \Big/ m_h + m_e\right) \quad (2a)$$

$$E_{vb} = E_{cb} - E_{g,observed} \quad (2b)$$

where $E_{g,bulk}$, $E_{g,observed}$, $E_{cb,bulk}$, m_h, and m_e are the bulk bandgap (CdSe ~ 1.74 eV), the observed bandgap as determined from the first absorption resonance energy, the bulk conduction band energy (versus vacuum), the effective hole mass (CdSe ~ 0.45), and the effective electron mass (CdSe ~ 0.13), respectively. Our experimental results show that the overall PL intensity of nanoparticles is considerably higher in ZrO_2 hosts than in TiO_2. The titania matrix ($E_{cb,TiO_2} \simeq$ –4.06 eV at pH 7)[32] quenches the QD fluorescence. This cannot be caused by charge-carrier diffusion into the matrix if we accept the low E_{cb} values (–4.7 to –4.4 eV) in the literature. If however we utilize a typical $E_{cb,bulk}$ value of –4.3 eV (ca. –0.2 versus a normal hydrogen electrode (NHE)), as used by Nozik and Memming,[32] then electron emission into the titania matrix would be energetically feasible and the low luminescence QYs could be rationalized. We summarize our view of the relative disposition of the NC and matrix energy levels in Figure 6. Based upon these assumptions, QDs with a CdSe core diameter (first absolute maximum) of less than ca. 5.6 nm (ca. 620 nm) should in principle be readily quenched in titania matrices. Although this value is the lower limit, this rationale may explain why recent studies showed reasonable stability of CdSe lasing in titania hosts, particularly for larger particles and at low temperature (where an activation barrier may result in sluggish electron-transfer kinetics).[7,10] Unlike titania, which appears to exhibit size-dependent NC quenching, the small electron affinity of zirconia ($E_{cb,ZrO_2} \simeq$ –3.00 eV)[31] prevents charge transfer entirely. This suggests that the ZrO_2 matrix is a much more appropriate host for CdSe QDs of all sizes.

The results presented here demonstrate that optimization of the waveguiding properties involves a compromise with the annealing temperature. Low-temperature treatment allows the composites to retain maximum PL activity, but only very low n_g values are achieved. However at the highest treatment temperature, no PL is observed, but the matrix attains the highest n_g values. Our results indicate that the optimal annealing temperature range for CdSe–ZnS NCs in zirconia lies between 200 and 300 °C.

2.4. Waveguide Propagation

The importance of maximizing the matrix refractive index is clear from the cutoff condition of the fundamental transverse electric (TE) mode in an asymmetric waveguide, which consists of a thin guiding layer on a substrate, in air[43]

$$\frac{d}{\lambda_0} = \frac{1}{2\pi\sqrt{n_g^2 - n_s^2}} \tan^{-1}\sqrt{\frac{n_s^2 - 1}{n_g^2 - n_s^2}} \quad (3)$$

Here n_g and n_s are the refractive indices of the guiding layer and substrate, respectively, while d and λ_0 are the thickness of the guiding layer and the propagation wavelength in a vacuum, respectively. This equation implies that a large difference in the refractive-index value between the guiding layer and the substrate, will reduce the required minimum d/λ_0 ratio to observe mode propagation. To show this, we include the value of the minimum d/λ_0 ratio in Table 1 for the experimentally obtained n_g values at each annealing step for a film deposited on a fused silica substrate, where $n_{s,633\ nm} \simeq 1.45$. The advantage of high-refractive-index waveguide materials is also important for maximizing the power stored in the guiding layer. This is described by the so-called confinement factor and is defined as the fraction of the modal power confined within the guiding layer. Although no simple analytical expression for this factor

exists, it is evident that for a constant d value, a higher refractive-index difference between the guide and substrate layer results in an increased localization of the modal electric field within the guiding layer, and hence gives rise to a higher confinement factor. For a detailed description the reader is referred to any standard textbook on waveguides[44–46].

Experimentally, the simplest method of determining the allowed modes in a waveguide structure is through the use of a prism-coupling technique usually termed the m-line method.[45] Here we performed such m-line measurements under TE conditions on multilayer (×3) thin-films (heat-treated up to 300 °C) deposited on fused silica ($n_{r,633\ nm} \simeq 1.45$). The results are shown in Figure 7a and b for the QD-TiO_2 and QD-ZrO_2 composites, respectively. Single-mode propagation (TE_0) was confirmed in each case, demonstrating that both matrices could be utilized as effective waveguides. It should be noted that multimode waveguides can be easily fabricated by increasing the number of deposited layers.

To measure the optical losses within such waveguides, doped and undoped ZrO_2 films with thicknesses of ca. 400–500 nm were prepared and tested with the technique described by Nunzi Conti et al.[47] The high absorption of the QDs induces a high value of the attenuation coefficient of the waveguides in the visible, not making this parameter indicative of the actual optical quality of the films. For this reason we measured the attenuation coefficients in the near-infrared (NIR) region (1.542 μm), where the effect caused by QD absorption is not so crucial. The large increase in waveguide thickness necessary to support modes in the NIR also induces a large number of macroscopic defects and inhomogeneities, particularly caused by film deposition being carried out in non-clean-room conditions. In any case, for the waveguide with the ZrO_2-300 matrix we obtain an attenuation coefficient of (2.6 ± 0.3) dB cm^{-1} at 1542 nm and (1.7 ± 0.3) dB cm^{-1} at 632.8 nm. The higher attenuation at 1542 than at 632.8 nm is observed because of a lower confinement of radiation. For the waveguide with the ZrO_2-QD-300 matrix we obtain an attenuation coefficient of (1.7 ± 0.3) dB cm^{-1} at 1542 nm and (1.8 ± 0.3) dB cm^{-1} at 632.8 nm. In this case a slightly higher attenuation coefficient is observed at 632.8 nm owing to quantum dot reabsorption. The comparable attenuation coefficient values of both doped and undoped waveguides indicate that the nanoparticle inclusions do not have a detrimental effect on the waveguide quality; an observation supported by the surface roughness measurements.

Bawendi and co-workers have recently used heavily doped silica as a waveguiding substrate.[8,48] Like ZrO_2 ($E_g = 5.68$ eV), silica is a wide-bandgap insulator ($E_{g,SiO_2} \sim 7$–9 eV), with a fully densified refractive index of ca. 1.45 at 633 nm. ZrO_2 composites have a refractive index of ca. 0.15 less than TiO_2 hosts, but significantly higher than silica composites. This implies that unlike silica composites, which require high doping levels for waveguiding on glass (borosilicate, fused silica, quartz, etc.), ZrO_2 hosts can be deposited directly onto glass as waveguiding media.

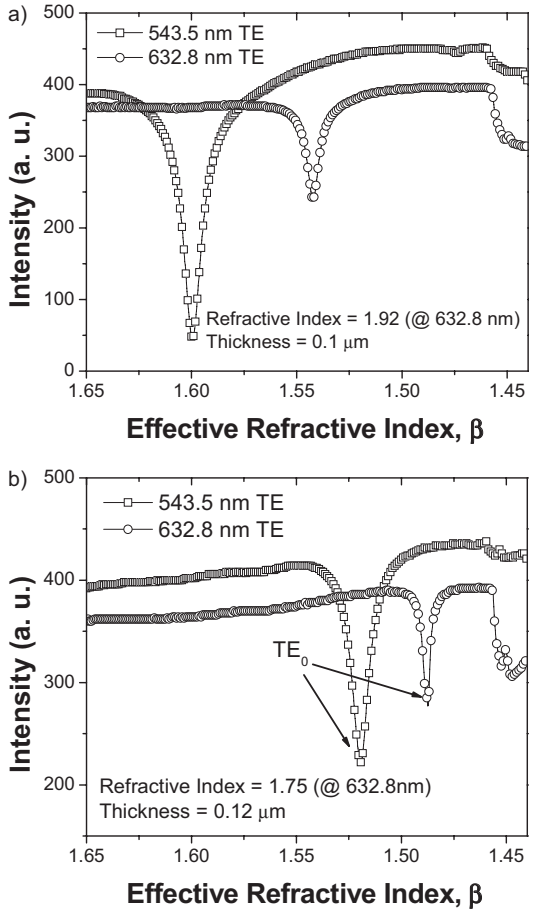

Figure 7. M-line measurements of TiO_2-QD (a) and ZrO_2-QD (b) composites as measured at 632.8 and 543.5 nm under TE polarization.

2.5. Photostability of Spontaneous and Amplified Stimulated Emission

To investigate the photostability within the films we compared the effects of excitation with i) a continuous-wave 488 nm source and ii) a repetition rate of 1 kHz with 150 fs 400 nm pulses (described further in the Experimental section). The continuous-wave excitation primarily targets the decay of single excitons within the QD volume whereas the pulsed setup accesses the multi-exciton regime. The results of continuous-wave excitation with an intensity of 35.3 kW cm^{-2} are shown in Figure 8. It is seen that after only 15 min of illumination, the initially normalized PL intensity of the QD-TiO_2 and QD-ZrO_2 composites drop to ca. 0.33 and ca. 0.84, respectively, of their original values.

It is known that for CdSe QDs a population inversion is obtained when the number of excitons in a given QD is greater than one.[6] This condition is easily satisfied under pulsed excitation, which, when utilized under fixed-stripe-length pumping conditions (see Experimental section), allows the stability of the ASE to be studied. The results for QD-TiO_2 and QD-ZrO_2 composites within this excitation regime (per pulse fluence of 0.32 mJ cm^{-2}) are displayed in Figure 9a and b. As expected, because both films had a similar QD fill-factor and thickness (ca. 200–300 nm), we observed ASE in both composites. The

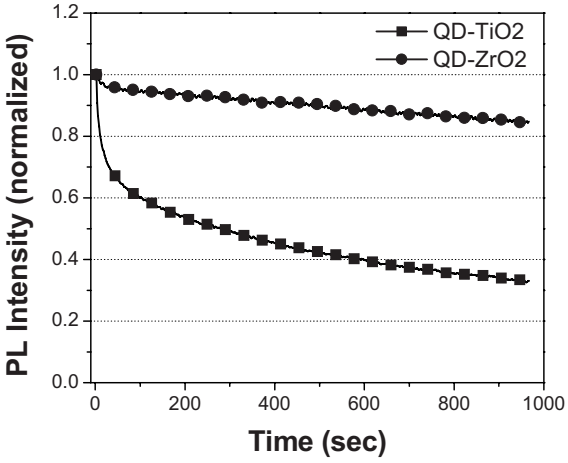

Figure 8. Fluorescence stability under continuous-wave 488 nm excitation with an excitation intensity of 35.3 kW cm^{-2}. The measurements were taken under a thin-film configuration with a laser confocal system in air and at room temperature.

observed difference between the stability of the two composites was however, staggering. The QD-TiO_2 ASE was displayed for less than 10 seconds in total, with 90 % of its value dropping within the first 3 s. In complete contrast, the ASE arising from the QD-ZrO_2 composite (shown in Fig. 9c) decreased by just 30 % of its original value after more than 40 min (2.4×10^6 pulses) excitation. This difference is again attributed to charge-carrier loss to the TiO_2 matrix. Interestingly, the ASE stability appeared to be more drastically affected than the spontaneous emission. This may indicate that Auger ionization, which occurs under multi-exciton conditions, is the dominant process governing photostability.[49] Critically, under both linear and nonlinear excitation regimes, the zirconia host provides a more stable matrix.

3. Conclusion

We have presented a comparative study of the optical properties of CdSe–ZnS QDs with a ca. 4.6 nm diameter core embedded within two high-refractive-index host matrices, TiO_2 and ZrO_2. The use of strongly chelated sol-precursors, obviated the need for large quantities of excess ligand in the sol–gel synthesis allowing nanoparticle–host interactions to be studied. Although both matrices were found to be suitable waveguide materials, the QD-ZrO_2 composites typically exhibited PL intensities 20–30 times greater than that of the QD-TiO_2 system. A comparison of the conduction-band offsets suggests electron transfer from the NC to the matrix as being the cause of this instability in QD-TiO_2 films. Furthermore high photostability in zirconia composites was observed under continuous-wave excitation, and one of the highest reported stability factors for ASE to date. Based on both the spontaneous and ASE we be-

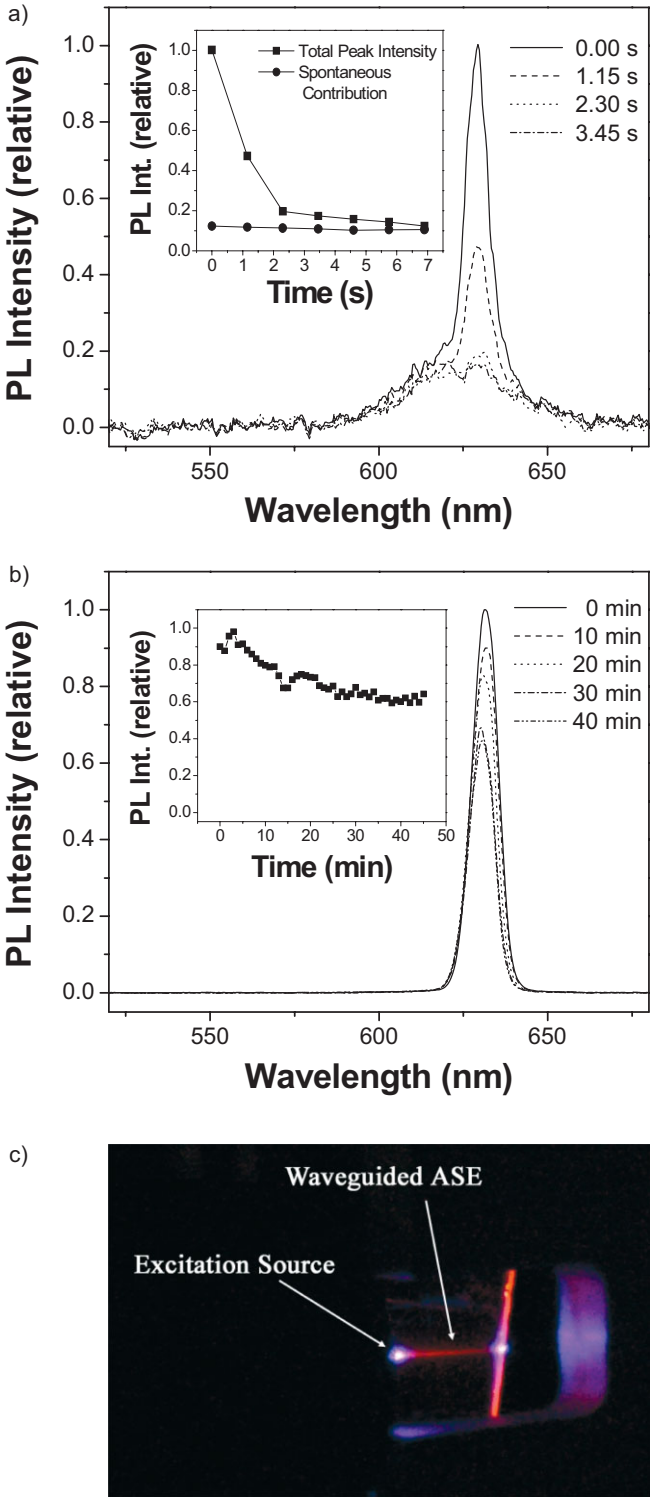

Figure 9. ASE stability of TiO_2-QD (a) and ZrO_2-QD (b) composites pumped at 400 nm with 150 fs pulses under a pump fluence of 0.32 mJ cm^{-2}. This excitation fluence is well within the multi-exciton regime for CdSe–ZnS nanoparticles. The stability is shown for samples in air at room temperature. c) A digital photograph of waveguided ASE in the ZrO_2-QD thin film.

ADVANCED FUNCTIONAL MATERIALS

lieve QD-ZrO_2 composites provide a superior functional material for optical-gain applications.

4. Experimental

5-Amino-1-pentanol (AP, 95 %), zirconium(IV) isopropoxide (70 wt % in 1-PrOH), titanium(IV) isopropoxide (97 %), acetylacetone (ACAC, 99 %) were purchased from Sigma–Aldrich. Hexane, chloroform, PrOH (propanol), EtOH (ethanol), and MeOH were all of analytical grade and purchased from Univar. All chemicals and solvents were used without further purification.

CdSe NC preparations were prepared by using established methods reported by van Embden et al. [50]. Shelling of the NCs was further performed using the recently developed SILAR method [26,51]. To render the NCs soluble in alcohol solutions, a similar procedure to that utilized by Petruska et al. was used [9]. The NCs were firstly precipitated from chloroform with AP. These NCs were then redispersed in a 1:1 mixture by volume of EtOH/$CHCl_3$ with 0.1 M AP to promote thorough ligand exchange. The solution was stirred gently for 12–24 h. Following this, the NCs were precipitated with excess hexane. The AP-functionalized particles were then redispersed in MeOH and were colloidally stable for a over 1 month.

The zirconia sol was prepared in a similar manner to that used by Urlacher et al., by mixing $Zr(OPr)_4$ (1 mL, 2.26 mmol), acetylacetone (acac) (0.23 mL, 2.26 mmol), and i-PrOH (6 mL) [52]. The titania sol was prepared in a very similar fashion by mixing $Ti(OPr)_4$ (0.64 mL, 2.26 mmol), acac (0.23 mL, 2.26 mmol), and i-PrOH (6.4 mL). To ensure chelation of the metal cations by acac, each sol-solution was stirred for ca. 1 h prior to their use. Thin-films consisting of pure titania or zirconia were obtained by spin-coating the sol-solutions on precleaned substrates (fused silica, borosilicate glass, or silicon substrates). QD-doped thin films were produced by adding 100 μL of sol–gel sol-solution to 200 μL of a 74 μM solution of QDs in MeOH. The molar ratio of QDs to titania or zirconia was kept the same for both composites. All the films in this study were spin-coated at 3500 rpm for 20 s. Heat-treatment of the films took place between 100 and 500 °C, with a 100 °C temperature interval and 5 min annealing time at each temperature. TEM of QDs in TiO_2 and ZrO_2 was performed on films that were spin-coated at 6000 rpm directly onto a strong, carbon-coated copper grid and annealed at 100 °C for 15 min. M-line measurements were performed on samples heated up to 300 °C. These were carried out on multilayer films annealed at 100, 200, and 300 °C for 5 min per layer on fused silica substrates.

Tapping-mode AFM measurements were performed on a Veeco Dimension 3100 using Budgetsensor cantilevers (spring constant, $k_0 = 40\ N\ m^{-1}$). TEM measurements were carried out on a Philips BioTwin instrument operating at 120 keV. Absorbance and PL spectra in solution were collected with a Cary 5 UV-vis-NIR spectrometer and a Varian Eclipse, respectively. PL and the temporal stability of spontaneous emission of the QD thin films were obtained using an Olympus FV500 laser-scanning confocal microscope coupled to a Triax 550 Jobin-Yvon spectrometer with a liquid-nitrogen-cooled charge-coupled device (CCD). The excitation source was an Ar^+ laser operating at 488 nm. A 20 × 0.7 numerical aperture (NA) objective (Olympus) was used to excite and collect the PL for heat-treatment studies and a 40 × 1.0 NA oil-immersion objective (Olympus) was used in the PL stability measurements. ASE was produced with a 1 kHz 150 fs pulsed frequency-doubled Ti:Sapphire laser under a 1D amplifier configuration. To measure the stability we used a variable-string-length configuration where we fixed the pump length to 0.2 cm [53]. The edge-coupled waveguided light was perpendicular to the excitation source and was detected by using an optical fiber connected to an Ocean Optics micro-spectrometer. M-line measurements were carried out using a HeNe laser at 632.8 and at 543.5 nm under TE polarization using a standard prism-coupling technique. Ellipsometry measurements were taken on a Jobin–Yvon Uvisel spectroscopic ellipsometer.

Received: October 13, 2006
Revised: February 8, 2007
Published online: May 9, 2007

[1] S. T. Selvan, C. Bullen, M. Ashokkumar, P. Mulvaney, *Adv. Mater.* **2001**, *13*, 985.
[2] C. Li, N. Murase, *Langmuir* **2004**, *20*, 1.
[3] K. Yang, H. Fan, K. J. Malloy, C. J. Brinker, T. W. Sigmon, *Thin Solid Films* **2005**, *491*, 38.
[4] J. Vejpravová, V. Sechovský, J. Plocek, D. Nižňanský, A. Hutlová, J.-L. Rehspringer, *J. Appl. Phys.* **2005**, *97*, 124 304.
[5] F. Bentivegna, J. Ferré, M. Nývlt, J. P. Jamet, D. Imhoff, M. Canva, D. Brun, P. Veillet, Š. Višňovský, F. Chaput, J. P. Boilot, *J. Appl. Phys.* **1998**, *83*, 7776.
[6] V. I. Klimov, A. A. Mikhailovsky, S. Xu, A. Malko, J. A. Hollingsworth, C. A. Leatherdale, H. J. Eisler, M. G. Bawendi, *Science* **2000**, *290*, 314.
[7] H.-J. Eisler, V. C. Sundar, M. G. Bawendi, M. Walsh, H. I. Smith, V. Klimov, *Appl. Phys. Lett.* **2002**, *80*, 4614.
[8] Y. Chan, J. S. Steckl, P. T. Snee, J. M. Caruge, J. M. Hodgkiss, D. G. Nocera, M. G. Bawendi, *Appl. Phys. Lett.* **2005**, *86*, 073 102.
[9] M. A. Petruska, A. V. Malko, P. M. Voyles, V. I. Klimov, *Adv. Mater.* **2003**, *15*, 610.
[10] V. C. Sundar, H.-J. Eisler, M. G. Bawendi, *Adv. Mater.* **2002**, *14*, 739.
[11] M. A. Petruska, A. P. Bartko, V. I. Klimov, *J. Am. Chem. Soc.* **2004**, *126*, 714.
[12] K. R. Choudhury, Y. Sahoo, P. N. Prasad, *Adv. Mater.* **2005**, *17*, 2877.
[13] J. Lee, V. C. Sundar, J. R. Heine, M. G. Bawendi, K. F. Jensen, *Adv. Mater.* **2000**, *12*, 2.
[14] Y. K. Olsson, G. Chen, R. Rapaport, D. T. Fuchs, V. C. Sundar, J. S. Steckel, M. G. Bawendi, A. Aharoni, U. Banin, *Appl. Phys. Lett.* **2004**, *85*, 4469.
[15] S. Pelli, G. C. Righini, A. Scaglione, M. Guglielmi, A. Martucci, *Opt. Mater.* **1996**, *5*, 119.
[16] Y. Sorek, M. Zevin, R. Reisfeld, T. Hurvits, S. Ruschin, *Chem. Mater.* **1997**, *9*, 670.
[17] T. Saraidarov, R. Reisfeld, M. Kazes, U. Banin, *Opt. Lett.* **2006**, *31*, 356.
[18] J. Bellesa, S. Rabate, J. C. Plenet, J. Dumas, J. Mugnier, O. Marty, *Appl. Phys. Lett.* **2001**, *79*, 2142.
[19] A. Martucci, A. Chiasera, M. Montagna, M. Ferrari, *J. Non-Cryst. Solids* **2003**, *322*, 295.
[20] C. Bullen, P. Mulvaney, C. Sada, M. Ferrari, A. Chiasera, A. Martucci, *J. Mater. Chem.* **2004**, *14*, 1112.
[21] A. Martucci, P. Innocenzi, J. Fick, J. D. Mackenzie, *J. Non-Cryst. Solids* **1999**, *244*, 55.
[22] V. Ptatschek, B. Schreder, K. Herz, U. Hilbert, W. Ossau, G. Schottner, O. Rahauser, T. Bischof, G. Lermann, A. Materny, W. Kiefer, G. Bacher, A. Forchel, D. Su, M. Giersig, G. Muller, L. Spanhel, *J. Phys. Chem. B* **1997**, *101*, 8898.
[23] F. L. Pedrotti, L. S. Pedrotti, *Introduction to Optics*, 2nd ed., Prentice-Hall, Englewood Cliffs, NJ **1993**.
[24] C. B. Poitras, M. Lipson, H. Du, M. A. Hahn, T. D. Krauss, *Appl. Phys. Lett.* **2003**, *82*, 4032.
[25] S. Rabate, J. Bellesa, C. Bonnand, J. C. Plenet, L. Spanhel, *Eur. Phys. J. B* **2004**, *42*, 47.
[26] R. Xie, K. Kolb, J. Li, T. Basché, A. Mews, *J. Am. Chem. Soc.* **2005**, *127*, 7480.
[27] D. E. Gomez, J. van Embden, J. Jasieniak, T. A. Smith, P. Mulvaney, *Small* **2006**, *2*, 204.

[28] L. Manna, C. Scher Erik, L.-S. Li, A. P. Alivisatos, *J. Am. Chem. Soc.* **2002**, *124*, 7136.
[29] T. D. Krauss, S. O'Brien, L. E. Brus, *J. Phys. Chem. B* **2001**, *105*, 1725.
[30] J. L. Blackburn, D. C. Selmarten, A. J. Nozik, *J. Phys. Chem. B* **2003**, *107*, 14 154.
[31] S. Sayan, R. A. Bartynski, X. Zhao, E. P. Gusev, D. Vanderbilt, M. Croft, M. Banaszak Holl, E. Garfunkel, *Phys. Status Solidi B* **2004**, *241*, 2246.
[32] A. J. Nozik, R. Memming, *J. Phys. Chem.* **1996**, *100*, 13 061.
[33] D. A. G. Bruggeman, *Ann. Phys.* **1935**, *24*, 636.
[34] W. D. Kingery, H. K. Bowen, D. R. Uhlmann, *Introduction to ceramics*, 2nd ed., Wiley, New York **1976**.
[35] R. H. French, S. J. Glass, F. S. Ohuchi, Y.-N. Xu, W. Y. Ching, *Phys. Rev. B: Condens. Matter Mater. Phys.* **1994**, *49*, 5133.
[36] C. J. Brinker, G. W. Scherer, *Sol–Gel Science: The Physics and Chemistry of Sol–Gel Processing*, Academic, San Diego, CA **1990**.
[37] E. Kucur, J. Riegler, G. A. Urban, T. Nann, *J. Chem. Phys.* **2003**, *119*, 2333.
[38] C. Wang, M. Shim, P. Guyot-Sionnest, *Science* **2001**, *291*, 2390.
[39] S. Coe, W.-K. Woo, M. Bawendi, V. Bulovic, *Nature* **2002**, *420*, 800.
[40] A. H. Mueller, M. A. Petruska, M. Achermann, D. J. Werder, E. A. Akhadov, D. D. Koleske, M. A. Hoffbauer, V. I. Klimov, *Nano Lett.* **2005**, *5*, 1039.
[41] C. Burda, T. C. Green, S. Link, M. A. El-Sayed, *J. Phys. Chem. B* **1999**, *103*, 1783.
[42] C. Querner, P. Reiss, S. Sadki, M. Zegorska, A. Pron, *Phys. Chem. Chem. Phys.* **2005**, *7*, 3204.
[43] H. Kogelnik, V. Ramaswamy, *Appl. Opt.* **1974**, *13*, 1857.
[44] A. Yariv, *Quantum Electronics*, Wiley, New York **1989**.
[45] R. Syms, J. Cozens, *Optical Guided Waves and Devices*, McGraw-Hill, London **1992**.
[46] A. W. Snyder, J. Love, *Optical Waveguide Theory*, Chapman and Hall, London, **1983**.
[47] G. Nunzi Conti, A. Chiasera, M. Brenci, M. Ferrari, S. Pelli, S. Sebastiani, C. Tosello, G. C. Righini, *J. Non-Cryst. Solids* **2006**, *352*, 2585.
[48] Y. Chan, P. T. Snee, J. M. Caruge, B. K. Yen, G. P. Nair, D. G. Nocera, M. G. Bawendi, *J. Am. Chem. Soc.* **2006**, *128*, 3146.
[49] D. I. Chepik, A. L. Efros, A. I. Ekimov, M. G. Ivanov, V. A. Kharchenko, I. A. Kudryavtsev, T. V. Yazeva, *J. Lumin.* **1990**, *47*, 113.
[50] J. van Embden, P. Mulvaney, *Langmuir* **2005**, *21*, 10 226.
[51] J. J. Li, Y. A. Wang, W. Guo, J. C. Keay, T. D. Mishima, M. B. Johnson, X. Peng, *J. Am. Chem. Soc.* **2003**, *125*, 12 567.
[52] C. Urlacher, C. M. De Lucas, J. Mugnier, *Synth. Met.* **1997**, *90*, 199.
[53] K. L. Shaklee, R. R. Nahory, R. F. Leheny, *J. Lumin.* **1973**, *7*, 284.